

Structure of nanocomposites of Al–Fe alloys prepared by mechanical alloying and rapid solidification processing

S S NAYAK[†], B S MURTY^{††} and S K PABI*

Department of Metallurgical and Materials Engineering, Indian Institute of Technology, Kharagpur 721 302, India

[†]Presently a Research Associate at the University of Louisiana at Lafayette, Lafayette 70504, Louisiana, USA

^{††}Department of Metallurgical and Materials Engineering, Indian Institute of Technology Madras, Chennai 600 036, India

Abstract. Structures of Al-based nanocomposites of Al–Fe alloys prepared by mechanical alloying (MA) and subsequent annealing are compared with those obtained by rapid solidification processing (RSP). MA produced only supersaturated solid solution of Fe in Al up to 10 at.% Fe, while for higher Fe content up to 20 at.% the nonequilibrium intermetallic Al₅Fe₂ appeared. Subsequent annealing at 673 K resulted in more Al₅Fe₂ formation with very little coarsening. The equilibrium intermetallics, Al₃Fe (Al₁₃Fe₄), was not observed even at this temperature. In contrast, ribbons of similar composition produced by RSP formed fine cellular or dendritic structure with nanosized dispersoids of possibly a nano-quasicrystalline phase and amorphous phase along with α -Al depending on the Fe content in the alloys. This difference in the product structure can be attributed to the difference in alloying mechanisms in MA and RSP.

Keywords. Nanocomposites; Al–Fe; mechanical alloying; rapid solidification; quasicrystalline.

1. Introduction

Al–Fe alloys are attractive for applications at temperatures beyond those normally associated with the conventional aluminum alloys. Alloying Al with Fe increases the high temperature strength due to the dispersion of second-phase particles (Froes *et al* 2001). Unfortunately, the equilibrium solubility of Fe in the Al lattice is very low, and it does not exceed 0.03% (All the compositions are in atomic % unless otherwise stated) (Kattner 1986). Hence, these alloys cannot be precipitation strengthened by conventional ageing treatments. The strengthening effect can be enhanced by increasing the solid solubility of Fe in the Al matrix by some nonequilibrium processing techniques, viz. rapid solidification processing (RSP) (Tonejc and Bonifasčić 1969; Young and Cline 1981; Riontino and Zanada 1994; Badan *et al* 1996), mechanical alloying (MA) (Huang *et al* 1990; Niu *et al* 1994; Mukhopadhyay *et al* 1995; Fadeeva and Leonov 1996; Kaloshkin *et al* 2002) and severe plastic deformation (SPD) (Senkov *et al* 1998). These non-equilibrium processing techniques can refine the microstructure of metals and alloys up to nanometer-level, and lead to the formation of metastable phases including supersaturated solid solutions. These novel constitutional and microstructural effects can enhance the physical and mechanical properties.

RSP, MA and SPD have been reported as tools for extension of Fe solubility in Al, so that the resultant supersaturated solid solution can lead to the formation of nanocrystalline precipitation strengthened structure after aging (Froes *et al* 2001). In particular, MA and RSP of metallic alloys of many systems lead to the formation of materials with unique combination of advantageous properties, which are determined by the novel features of the microstructure and crystal structure of the alloys. No systematic comparison of the structure and morphology of the phases formed by MA and RSP in the Al-rich Al–Fe alloys of similar composition have been reported, so far. The present work attempts to fill this gap reporting a comparison of the structures of nanocomposites of Al–Fe alloys prepared by MA and subsequent annealing with those generated by RSP. This is of particular interest for the development of nanocomposites of this alloy system for high strength applications.

2. Experimental

2.1 Mechanical alloying (MA)

MA of Al–Fe alloys with nominal composition, Al_{100-x}Fe_x, for $x = 2.5, 5, 10, 15$ and 20 , was carried out using high purity powders of Al (99.9 wt.%) and Fe (99.98 wt.%) as the starting materials. Elemental powder blends of desired nominal composition were ball milled in a high energy Fritsch Pulverisette-5 planetary ball mill in cemented

*Author for correspondence (skpabi@metal.iitkgp.ernet.in)

carbide grinding media at a mill speed of 300 rpm and ball to powder ratio 10:1, using toluene as the process control agent. The as-milled powder samples were characterized by X-ray diffraction (XRD) for the phase identification and crystallite size measurements using the Co-K α radiation in a PHILIPS 1719 diffractometer. The effective crystallite size was calculated from the line profile analysis of Al(111) peak, recorded using Co-K α radiation, by the Voigt's equation after eliminating contribution of instrumental broadening as reported earlier (De Keijser *et al* 1982; Datta *et al* 2000a). The enthalpy of formation (ΔH_f) of Al-Fe alloys was calculated through Miedema's semiempirical model (De Boer *et al* 1989).

Nanocrystalline Al-Fe alloy powders after MA were consolidated into cylindrical pellets of 12 mm diameter under a load of 375 MPa for 15 s using an INSMART uniaxial hydraulic press. The density of the pellets was measured by the Archimedes' principle using the Sartorius density measurement kit. The consolidated pellets were characterized by PHILIPS X'pert Pro high resolution XRD using Cu-K α radiation for phase analysis. Microstructural analysis of the consolidated pellets was carried out by means of a PHILIPS CM30 transmission electron microscope (TEM) operated at 300 kV. For electron transparency, thin-foil specimens were mechanically polished and subsequently ion beam milled.

2.2 Rapid solidification processing (RSP)

Binary alloys of nominal compositions similar to those used in MA (see §2.1), i.e. Al-2.5, 5, 10, 15 and 20% Fe were prepared by melting appropriate amounts of high purity, Al (99.96%) and Fe (99.98%), under argon atmosphere in a high-frequency induction furnace. Melting of the alloys was carried out in a graphite crucible coated with boron nitride on its inner surface in order to minimize the contamination in the master alloys during melting. RSP of the molten alloys was carried out by a single-roller melt spinner with copper wheel of 300 mm diameter at different linear wheel speeds, viz. 20 m/s, 30 m/s and 40 m/s. The cooling rates were estimated to be in the range of 10^4 – 10^5 K/s. The melt-spun ribbons were about 1.5–3 mm wide and 25–100 μ m thick. The structural characterization of the as-spun alloys was carried out by XRD in a Rigaku CN-2301 diffractometer for the phase identification and lattice parameter measurements using monochromatic Cu-K α radiation. TEM of the melt-spun alloys was carried out for observing the microstructure and recording electron diffraction pattern using a JEOL 2000 FXII transmission electron microscope equipped with a Link energy-dispersive X-ray spectroscopy. For electron transparency, the thin-foil specimens were prepared by ion beam milling.

3. Results and discussion

3.1 Nanocomposites produced by MA

XRD analysis of all the compositions studied in the present work formed supersaturated solid solution of Fe in Al, i.e. Al(Fe) after 20 h of MA, except in the case of Al-20 %Fe alloy that formed the metastable Al₅Fe₂ intermetallic along with Al(Fe), as shown in figure 1(a). It was observed from these XRD patterns that after 20 h of MA, the intensity of Al(111) peak continuously decreased with concurrent increase in the peak width with Fe enrichment in the alloys. An increase in the XRD peak widths following milling under identical conditions increased with Fe content in the alloy, which indicated enhanced crystal size refinement during MA with Fe addition. This was confirmed from the variation of crystallite size of Al with Fe content in the alloy (figure 1(b)). The crystallite size after 20 h of MA was highest (27 nm) in the Al-2.5 %Fe alloy while a minimum crystallite size of 9 nm was measured for Al-20 %Fe alloy. Precise lattice parameter estimated from the patterns in figure 1(a) evidenced a shift of the Al(111) peak to higher diffraction angle with the increase in Fe content in the alloy up to 10% Fe (figure 1(b)), and this suggested the incorporation of more Fe atoms (0.124 nm dia.) into Al (0.143 nm dia.) lattice. However, beyond 10 %Fe the lattice parameter variation manifested a discontinuity and an increase with the addition of Fe (cf. for 15 and 20 %Fe in figure 1(b)), possibly evidencing the formation of a new phase.

While the intensity of Al(111) peak was found to decrease with increase in Fe content in the alloys, that of Al(200) peak increased and shifted to lower diffraction angle. In fact, Al-20 %Fe alloy after 20 h of MA was found to form a broad peak in the diffraction angle range 50–54 degree, and another shoulder peak was seen close to it indicating the contribution of another phase to the intensity of this peak (figure 1(a)). To ascertain the phases present in Al-20% Fe, the Al(200) peak profile was subjected to deconvolution, which is shown in figure 1(c). After this deconvolution, Al(200) and Al₅Fe₂(311) peaks were identified, however, the intensity of the Al(200) peak was low. The reason for decrease in Al(111) peak is the formation of more amounts of Al₅F₂ intermetallic during MA as the composition reached closer to its stoichiometric composition. The increase in intensity of Al(200) peak is attributed to overlapping of diffraction angle of Al(200) peak, Fe(110) peak from any undissolved Fe, as well as, of the Al₅F₂ (311) peak, so that they all contribute to form a broad peak due to the finer crystallite size after 20 h of MA. The intensity ratio of Al(200) peak in said deconvoluted pattern decreased with the increase in the Fe content in the alloy, suggesting the formation of Al₅F₂ intermetallic phase at the expense of Al (Nayak *et al* 2006; Nayak 2007).

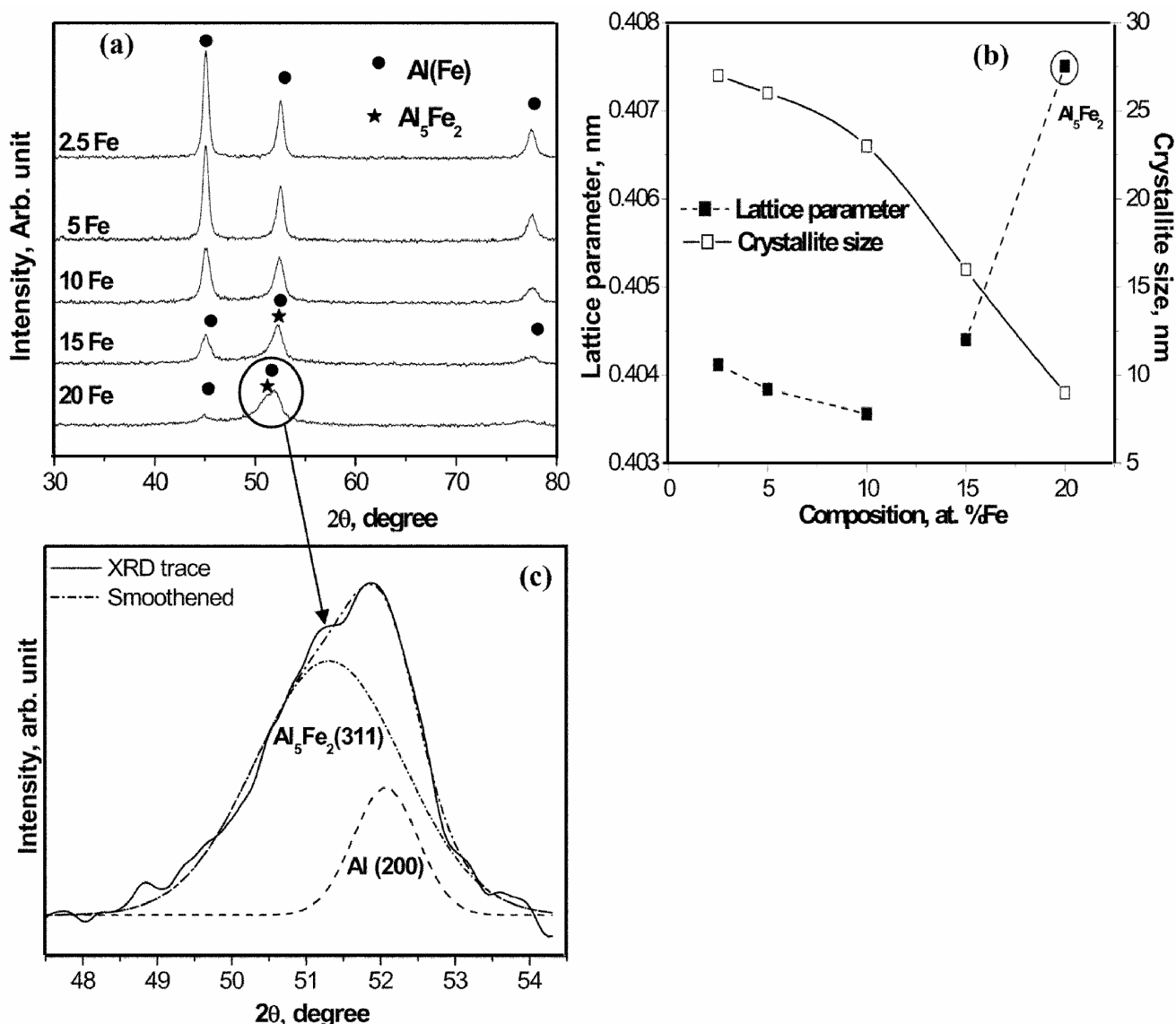


Figure 1. (a) XRD patterns of Al-Fe alloys after 20 h MA, (b) variation of lattice parameter and crystallite size as a function of Fe content in Al-Fe alloys estimated from patterns in (a). The encircled peak of Al-20%Fe alloy in (a) deconvoluted in (c) to show presence of Al₅Fe₂(311) and Al(200) in Al-20 %Fe after 20 h MA.

According to the phase diagram (Kattner 1986), all the alloy compositions studied in the present work should contain Al and Al₃Fe phases under equilibrium. It is interesting to note from figure 1 that under the present MA conditions, formation of Al₅Fe₂ intermetallic prevailed over the synthesis of equilibrium Al₃Fe phase in Al-20 %Fe alloy, which had a composition away from the stoichiometric composition of Al₃Fe. The reason for preferred formation of Al₅Fe₂ intermetallic can be attributed to the non-equilibrium nature of the MA process. The enthalpy of formation of Al₅Fe₂ ($\Delta H_f = -28.1$ kJ/mol) and Al₃Fe ($\Delta H_f = -28.26$ kJ/mol) calculated through the Miedema's semi-empirical model (De Boer *et al* 1989) are similar. Therefore, it is plausible that unlike Al₃Fe,

the Al₅Fe₂ being a congruent melting compound in the equilibrium diagram (Kattner 1986), is easier to form during MA or subsequent annealing (Datta *et al* 2000b). From the metastable phase diagram of the Al-Fe reported by other investigators (Adam and Hogan 1972; Fadeeva and Leonov 1996), the alloys containing more than 15 %Fe are expected to contain some Al₆Fe phase. In the present work, the formation of this metastable phase was also not observed, besides the formation of Al₃Fe being suppressed, which can be attributed to the large deviation from equilibrium during the MA process.

Figure 1(b) shows that beyond 10 %Fe the lattice parameter increased sharply giving a high value of 0.40751 nm in case of Al-20 %Fe, as marked by circle in the figure.

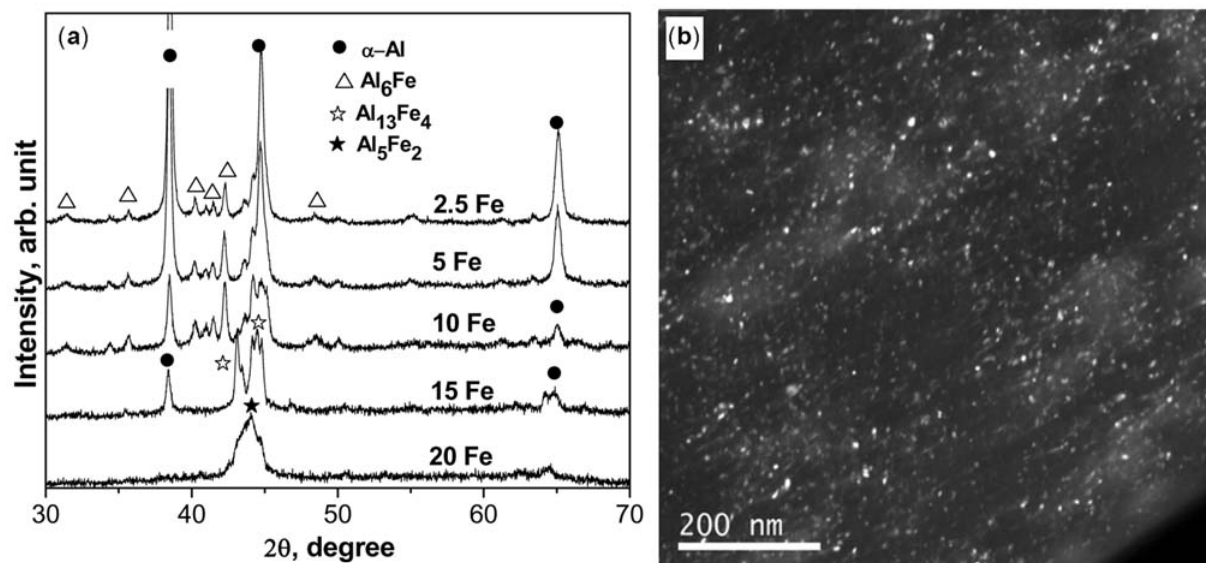


Figure 2. (a) XRD patterns of consolidated nanocrystalline Al-Fe alloys after annealing for 2 h at 673 K and (b) dark field image of Al-20 %Fe nanocrystalline powder after annealing at 673 K for 2 h.

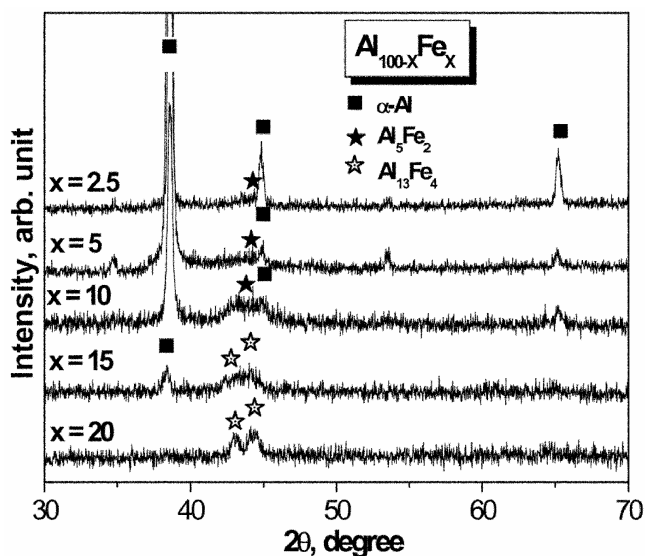


Figure 3. XRD patterns of $\text{Al}_{100-x}\text{Fe}_x$ alloys ($x = 2.5, 5, 10, 15$ and 20) melt spun at a linear wheel speed of 40 m/s.

Almost a single phase intermetallic Al_5Fe_2 formed in Al-20 %Fe alloy, which made the powder particle more brittle resulting in extreme refinement of the crystallites (9 nm) in this particular composition.

Annealing of the nanocrystalline dilute Al-Fe alloys containing 2.5–20 %Fe for 2 h at 673 K resulted in the formation of intermetallic phases along with the supersaturated solid solution of α -Al, as shown in the XRD patterns in figure 2(a). The type of intermetallic formed was found to be dependent on the Fe content, changing from Al_6Fe at 2.5–10 Fe to $\text{Al}_{13}\text{Fe}_4$ at 15 %Fe, while the

formation of Al_5Fe_2 possibly with some amount of amorphous phase was apparent only in the 20 %Fe composition. It may be recalled that after MA of Al-20 %Fe alloy for 20 h predominantly Al_5Fe_2 intermetallic was observed along with very small volume fraction of α -Al (figure 1(c)). The dark field image of the Al-20 %Fe nanocomposite powders after annealing at 673 K for 2 h confirmed the presence of bright nanocrystalline intermetallic particles as shown in figure 2(b). Here the grain size of ultra-fine intermetallic was measured to be around 15–20 nm indicating negligible grain growth from the starting size of 9 nm even after annealing at 673 K. It also confirmed the formation of nanocomposites of Al with metastable Al_5Fe_2 intermetallic in Al-20 %Fe alloy by MA and subsequent annealing at 673 K for 2 h.

3.2 Nanocomposites produced by RSP

Figure 3 shows the XRD patterns of $\text{Al}_{100-x}\text{Fe}_x$ ($x = 2.5, 5, 10, 15$ and 20) alloys melt spun at a linear wheel speed of 40 m/s. The Al-2.5 %Fe melt spun alloy was mostly single phase supersaturated solid solution of Fe in Al, as evident from the XRD pattern. The Al_5Fe_2 intermetallic appeared to be the second phase in Al-2.5%, Al-5 %Fe and Al-10 %Fe alloys. The most intense diffraction peak (311) of Al_5Fe_2 intermetallic phase was found at $2\theta = 43.79$ degree, which was quite close to Al (200) diffraction peak (44.73 degree) and hence, it was difficult to distinguish them in the patterns. In case of Al-15 %Fe alloy, the XRD peaks could be indexed as α -Al and $\text{Al}_{13}\text{Fe}_4$ phases, as shown in the patterns; while mostly single phase $\text{Al}_{13}\text{Fe}_4$ intermetallic was found in as melt spun Al-20 %Fe alloy. The volume fraction of $\text{Al}_{13}\text{Fe}_4$ increases with in-

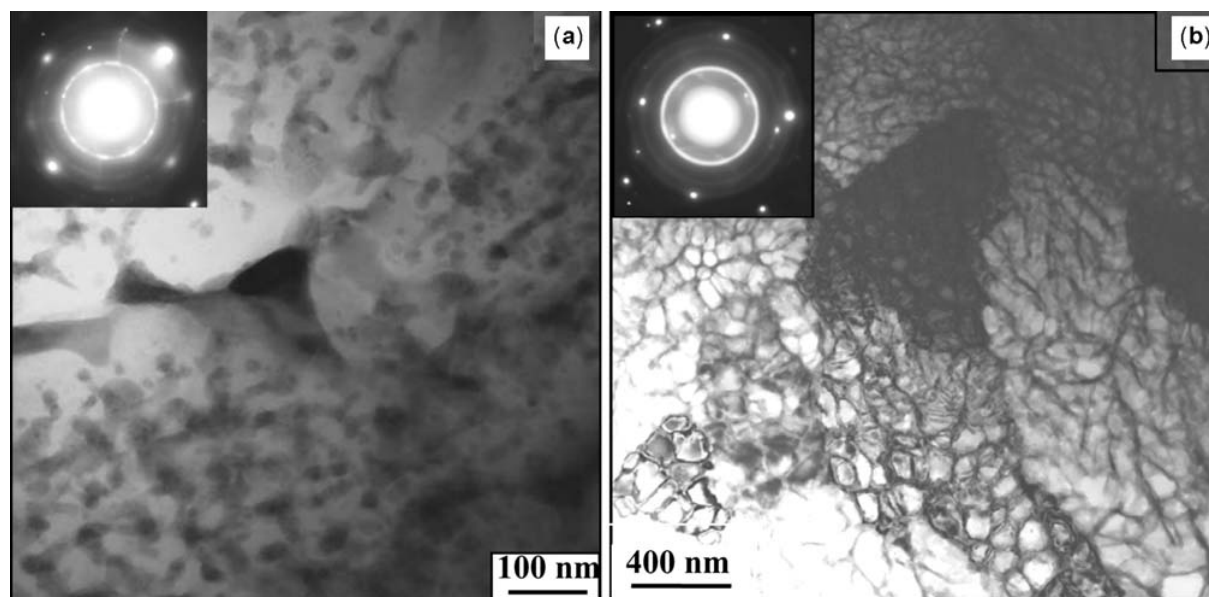


Figure 4. Bright field images of (a) Al–2.5 %Fe and (b) Al–5 %Fe alloy melt spun at a linear wheel speed of 40 m/s.

crease in Fe content of the alloy, as evident from the XRD patterns. The broadened XRD peaks indicate refinement of microstructure in these alloys due to the high cooling rate in melt spinning.

In the Al–Fe phase diagram (Kattner 1986), intermetallics with very complex crystal structures form and their most intense peaks are very close to the diffraction angle of Al(200) peak making it difficult to clearly identify them in the XRD analysis. To confirm the presence of the metastable phases in the melt spun alloys, a detailed TEM and electron diffraction (ED) study was carried out. Figures 4(a) and (b) show the microstructures of Al–2.5 %Fe and Al–5 %Fe alloys melt spun at a linear wheel speed of 40 m/s, respectively.

Dark regions of ultra-fine precipitates embedded in the bright α -Al matrix were found in the melt spun Al–2.5 %Fe alloy as shown in figure 4(a). Most of the precipitates here are < 20 nm in size, though some bigger precipitates possibly at the grain boundaries were also present in the microstructure. The nature of precipitates could not be clearly identified in TEM, since the nano-beam diffraction patterns could not be obtained from these precipitates. However, indexing of the ED pattern in figure 5(a) indicated that these precipitates structurally resemble some nanoquasicrystalline (NQ) phase (Nayak *et al* 2006; Nayak 2007). There are several reports on the formation of quasicrystalline phase in binary alloys containing at least 10% transition metal (TM) in Al (Shechtman *et al* 1984; Brendersky 1985; Brancel Hainey 1986; Fung *et al* 1986; Kelton 1993; Laissardiere *et al* 2005). However, quasicrystalline phase formation has not been reported so far in such dilute Al–TM alloys containing ≤ 2.5 %Fe. Increasing the Fe content of the alloy to 5%

made the solidification microstructure microcellular in nature, as shown in figure 4(b). The cells were 100–150 nm in size. Cellular morphology is normally caused by the instability in diffusion layer surrounding the growing solid owing to the solute segregation during growth (Mullins and Seherka 1963). The ED pattern taken from the intercellular region shows the diffraction rings of typical quasicrystalline symmetry, as shown in the inset in figure 4(b), suggesting the presence of nano-quasicrystalline phase in this dilute binary alloy as well (Nayak *et al* 2006; Nayak 2007). The ED patterns in the inset of both figures 4(a) and (b) show spotty diffraction rings from the α -Al crystals, which were also present in the microstructure of the melt spun alloy, as also evident from the XRD patterns in figure 3.

Interestingly, the microstructures of Al–10 %Fe and Al–15 %Fe alloys were found to be similar to that of Al–5 %Fe alloy with nodular precipitates in Al matrix. In contrast, the melt spun Al–20 %Fe alloy did not form any metastable phase, as evidenced by the XRD pattern in figure 3. TEM investigation showed that melt spun Al–20 %Fe alloy formed dendrites of intermetallic phase, $\text{Al}_{13}\text{Fe}_4$, which is close to the composition of the equilibrium intermetallic phase, Al_3Fe (Kattner 1986).

Finally, comparison of the microstructures of the Al-rich Al–Fe alloys of identical composition after MA and RSP shows they are entirely different. This divergence can originate from the difference in the mechanism of non-equilibrium phase formation in these two processing routes. In RSP all the alloying elements are in solution in the liquid prior to rapid solidification and these along with thermal disorder are partly frozen-in to yield the resultant phases. On the other hand, the sequence of dissolution

and/or reaction of different alloying elements under the influence of deformation induced intermixing (Pabi and Murty 1996; Pabi *et al* 1998) and mechanical disorder induced in the MA process are likely to dictate the resultant phase evolution.

4. Conclusions

(I) Successful synthesis of nanocomposites of Al–Fe alloys containing 2.5, 5, 10, 15 and 20% Fe was achieved by two most commonly used non-equilibrium processing routes viz. MA and RSP.

(II) After MA for 20 h, alloys containing up to 10 %Fe showed the formation of supersaturated solid solution of Fe in Al form, while in the case of Al–20 %Fe alloy metastable Al_5Fe_2 intermetallic along with the super saturated solid solution was found.

(III) Formation of the equilibrium intermetallic phase, Al_3Fe , was not observed during MA and even after subsequent annealing at higher temperature (673 K), and the formation of the congruent melting intermetallic phase, Al_5Fe_2 , was favoured.

(IV) Annealing at 673 K for 2 h after MA resulted in only marginal coarsening of the grain size of the intermetallics from ~9 nm to 15–20 nm indicating the formation of true nanocomposite by this route.

(V) Some indication of a quasicrystalline related phase formation in the dilute binary Al–TM alloys containing 2.5 and 5 %Fe was noted.

(VI) Ultra-fine and possibly quasicrystalline precipitates, mostly < 20 nm in size, dispersed in the α -Al matrix were found in the melt spun Al–2.5 %Fe alloy. Increase in the Fe content of the alloy from 5–15% made the solidification microstructure microcellular in nature. Melt spun Al–20 %Fe alloy formed dendrites of intermetallic phase, $\text{Al}_{13}\text{Fe}_4$, which is close to the composition of equilibrium intermetallic phase, Al_3Fe .

(VII) The difference in observed microstructure of the present Al–Fe alloys obtained through the two non-equilibrium processing routes, i.e. MA and RSP, can be attributed to the difference in alloying mechanism in the two processes.

Acknowledgements

The present work is partly sponsored by the Department of Science and Technology (grant No. SR/S5/NM-S1/2002). Authors are thankful to Peter Schubert-Bischoff and Dagmar Köpnick-Welzel, Hahn-Meitner-Institut (HMI), Berlin, for their help in preparing the TEM samples for this work. (SSN) acknowledges Prof. J Banhart, HMI, Berlin, and Prof. D -H Kim, Yonsei University, Seoul,

South Korea, for providing him support for carrying out part of this work.

References

- Adam C M and Hogan L M 1972 *J. Aust. Inst. Met.* **17** 81
 Badan B, Margini M and Zambon A 1996 *Scr. Mater.* **35** 13
 Brancel P A and Heiney P A 1986 *Phys. Rev.* **B33** 7917
 Brendersky L 1985 *Phys. Rev. Lett.* **55** 1461
 Datta M K, Pabi S K and Murty B S 2000a *J. Mater. Res.* **15** 1429
 Datta M K, Pabi S K and Murty B S 2000b *J. Appl. Phys.* **87** 8393
 De Boer F R, Room R, Nattens W C M, Miedema A R and Niessen A K 1989 *Cohesion and structure* (eds) F R de Boer and D G Pettifor (Amsterdam: North Holland) **Vol. 1**, p. 38
 De Keijser T H, Langford J I, Mittemeijer E I and Vogels A B P 1982 *J. Appl. Crystallogr.* **15** 308
 Fadeeva V I and Leonov A V 1996 *Mater. Sci. Eng.* **A206** 90
 Froes F H, Senkov O N and Baburaj E G 2001 *Mater. Sci. Eng.* **A301** 44
 Fung K K, Yang C Y, Zhou Y Q, Zhao J G, Zhan W S and Chen B G 1986 *Phys. Rev. Lett.* **58** 2060
 Huang B, Tokizane N, Ishihara K N, Shingu P H and Nasu S 1990 *J. Non-Cryst. Solids* **117/118** 688
 Kaloshkin S D, Tcherdynstev V V, Tomlin A I, Gunderov D V, Stolyarov V V, Baldokhin Y V, Brodova G I and Shelekhov E V 2002 *Mater. Trans. JIM* **43** 2031
 Kattner U R 1986 in *Al–Fe, binary alloy phase diagrams* (ed.) T B Massalski (Metals Park, Ohio: American Society for Metals) **Vol. 1**, p. 147
 Kelton K F 1993 *Int. Mater. Rev.* **38** 105
 Laissardiere G T, Nguyen-Manh D and Mayou D 2005 *Prog. Mater. Sci.* **50** 679
 Mukhopadhyay D K, Suryanarayana C and Froes F H 1995 *Metall. Mater. Trans.* **A26** 1939
 Mullins W W and Sekerka R F 1963 *J. Appl. Phys.* **35** 444
 Nayak S S 2007 *Synthesis and characterization of nanocrystalline intermetallics and nanocomposites of Al–TM alloys (TM = Ti, Zr, Fe) prepared by non-equilibrium processing routes*, PhD Thesis, Indian Institute of Technology, Kharagpur
 Nayak S S, Kim D H, Pabi S K and Murty B S 2006 *Trans. Ind. Inst. Met.* **59** 193
 Niu X P, Froyen L, Delaey L and Peytour C 1994 *J. Mater. Sci.* **29** 3724
 Pabi S K and Murty B S 1996 *Mater. Sci. Eng.* **A214** 146
 Pabi S K, Das D, Mahapatra T K and Manna I 1998 *Acta Mater.* **46** 3501
 Riontino G and Zanada A 1994 *Mater. Sci. Eng.* **A179–180** 323
 Senkov O N, Froes F H, Stolyarov V V, Valiev R Z and Liu J 1998 *Scr. Mater.* **38** 1516
 Shechtman D, Blech I, Gratias D and Cahn J W 1984 *Appl. Phys. Lett.* **53** 1951
 Tonejc A and Bonefasčić A 1969 *Scr. Metall.* **3** 145
 Young R M K and Clyne T W 1981 *Scr. Metall.* **15** 1211